JOURNAL OF THERMOPHYSICS AND HEAT TRANSFER
Vol. 10, No. 4, October–December 1996

# High-Resolution Solutions of Stiff Chemically Reacting Flows

Jacob Krispin* and Harland M. Glaz†
*University of Maryland, College Park, Maryland 20742*
and
James P. Collins‡
*U.S. Naval Surface Warfare Center, Silver Spring, Maryland 20903-5000*

**The objective of this work is to develop a high-resolution scheme for the equations of gasdynamics with stiff source terms, such as found when modeling chemically reacting flows. We do this by modifying a Godunov-like, hybrid implicit–explicit scheme to handle both stiff and nonstiff source terms. This modification retains second-order accurate steady states. Innovative approaches for stiff source terms are implemented. The resulting scheme is applied to the equations for nonequilibrium, chemically reacting flows in two dimensions. Two unsteady problems are studied: 1) a doubly periodic, unstable, low Mach number shear-layer flow and 2) the simulation of the evolution of a shock wave caused from the transverse injection of fluid into supersonic flow. In both flowfields, and for several reaction models, the numerical results prove that the extended implicit–explicit methodology can handle complex flow problems and produce highly resolved solutions. We also found that our standard approach to nonstiff sources cannot handle stiff problems; even when using very small integration steps the solution becomes unstable and eventually breaks down.**

## Introduction

OUR work here is based on a hybrid implicit–explicit (IE) Godunov-like scheme for hyperbolic conservation laws. Here, the wave fields are decomposed and each field is treated either implicitly or explicitly according to user-defined Courant–Friedrichs–Lewy (CFL) criteria. For example, if the flowfield is nearly incompressible, then it is necessary to treat the particle characteristic field explicitly while the (low energy-containing) sonic modes can be treated implicitly with little loss in accuracy and a large gain in efficiency. This approach was introduced in the context of Lagrangian hydrodynamics[1] and has been recently extended to the Eulerian case, see Ref. 2 for the one-dimensional scheme and Refs. 3 and 4 for the two-dimensional unsplit scheme; the latter scheme is the basis for the present work.

The implicit–explicit approach addresses the issue of wave-speed stiffness, that is, problems for which high-speed waves restrict the explicit CFL time step. The present work is concerned with the problem of source-term stiffness that arises in, for example, reactive flow and/or two-phase flow. We study several new innovative approaches due to Yee et al.,[5–7] Pember,[8] and the present authors. Two problems are discussed. First, a low-speed reactive shear layer is studied using extensions of the implicit–explicit scheme; see Ref. 9 for preliminary work. Second, a high Mach number reactive flowfield is studied using extensions of the unsplit explicit scheme.

## Governing Equations

The equations for chemically reacting flow that we solve are

$$(\rho^\alpha)_t + \nabla\cdot(\rho^\alpha \boldsymbol{u}) = \dot{w}^\alpha$$

$$(\rho\boldsymbol{u})_t + \nabla\cdot(\rho\boldsymbol{u}\boldsymbol{u}^T + p) = 0$$

$$(\rho E)_t + \nabla\cdot(\rho\boldsymbol{u}E + \boldsymbol{u}p) = -\sum_\alpha \dot{w}^\alpha(\Delta h_f^0)^\alpha$$

$$(\rho^\alpha q^\alpha)_t + \nabla\cdot(\rho^\alpha q^\alpha \boldsymbol{u}) = \rho^\alpha \dot{q}^\alpha \qquad (1)$$

where $\alpha = 1, \ldots, N$, $\rho^\alpha$ = density of species $\alpha$, $\rho \equiv$ mixture density $= \Sigma_\alpha \rho^\alpha$, $\boldsymbol{u}$ = velocity, $p$ = pressure, $E$ = total energy per unit mass, $q^\alpha$ = vibrational energy per unit mass of species $\alpha$, $(\Delta h_f^0)^\alpha$ = specific heat of formation at 0 K of species $\alpha$, and $N$ = total number of species present. The source terms $\dot{w}^\alpha$ and $\dot{q}^\alpha$ represent the production of species $\alpha$ through chemical reaction and the relaxation of vibrational energy of species $\alpha$ to its equilibrium value, respectively. Note that relaxation of vibrational energy equations applies only to molecules.

The computer code used for the results presented herein is designed for a five-species, reacting air mixture consisting of $N_2$, $O_2$, NO, O, and N (Ref. 10); a switch is included so that results can also be obtained for the simplified system consisting of nonequilibrium vibrational relaxation (as indicated later), but frozen species conservation. The modifications required for the simplified model are obvious, and we omit their discussion. For the purposes of the current study, both models are sufficient to produce the necessary numerical stiffness. The full system is sufficient for realistic high-temperature simulations up to about 7000–8000 K. The extension to a more complete air model (e.g., 11 species), together with a two- or three-temperature model that better describes higher temperature regimes, is straightforward.

The pressure is given by the equation-of-state

$$p = \rho\bar{R}T$$

where $T$ = temperature, $\bar{R} = R/M$, $R$ = universal gas constant, $M = (\Sigma_\alpha c^\alpha/M^\alpha)^{-1}$, $M^\alpha$ = molecular weight of species $\alpha$, and $c^\alpha = \rho^\alpha/\rho \equiv$ mass fraction of species $\alpha$. The total specific energy is

$$E = e + \tfrac{1}{2}|\boldsymbol{u}|^2$$

where $e$ = specific internal energy of the mixture, i.e., $e = \Sigma_\alpha c^\alpha e^\alpha$ with $e^\alpha$ = specific internal energy of species $\alpha$:

$$e^\alpha = (\gamma^\alpha - 1)^{-1}R^\alpha T + q^\alpha$$

Received Jan. 26, 1994; revision received Jan. 9, 1996; accepted for publication Jan. 30, 1996. 

*Research Associate, Department of Mathematics. Member AIAA.
†Professor, Department of Mathematics. Associate Fellow AIAA.
‡Computer Scientist, Information and System Sciences Branch, 10901 New Hampshire Avenue.

Here, $R^\alpha = R/M^\alpha$ and $\gamma^\alpha$ = polytropic index for species $\alpha$ (=7/5 for diatomic species and 5/3 for monatomic species). The first term on the right-hand side (RHS) represents the contribution of translational and rotational modes (which are assumed to be in equilibrium), to the internal energy. Summing over $\alpha$ and solving for $T$ leads to

$$T = \left(e - \sum_\alpha c^\alpha q^\alpha\right) \Big/ \sum_\alpha \frac{c^\alpha R^\alpha}{\gamma^\alpha - 1}$$

Substituting the previous expression into the equation of state, one easily sees that the pressure is a function of the conserved quantities.

Conservation of mass implies that

$$\rho_t + \nabla \cdot (\rho \boldsymbol{u}) = 0$$

that is, $\Sigma_\alpha \dot{w}^\alpha = 0$. Note that $\Sigma_\alpha c^\alpha = 1$ and that only 11 of the 12 equations [given by the previous conservation of mass equation and conservation laws Eqs. (1)] are independent. When fully implicit, we solve the system Eqs. (1) only and the previous mass equation is not used. However, when the CFL number associated with the particle characteristic is explicit, we solve all 12 equations and use the extra equation to adjust the constraint on the mass fractions given above.

### Reaction Model

Following Ref. 11, we assume that the reaction mechanism consists of $R$ elementary reactions of the form

$$\sum_{\alpha=1}^{N} \nu'_{\alpha,r} X_\alpha \underset{k_{b,r}}{\overset{k_{f,r}}{\rightleftarrows}} \sum_{\alpha=1}^{N} \nu''_{\alpha,r} X_\alpha, \quad r = 1, \ldots, R$$

where $X_\alpha$ = molar concentration of species $\alpha$, $\nu'_{\alpha,r}$ and $\nu''_{\alpha,r}$ are the stoichiometric coefficients for species $\alpha$ in reaction $r$, and $k_{f,r}$ and $k_{b,r}$, which are experimentally determined explicit functions of $T$, are the forward and backward reaction rates, respectively. The production terms are[11]

$$\dot{w}^\alpha = M^\alpha \dot{X}_\alpha, \quad \alpha = 1, \ldots, N$$

where

$$\dot{X}_\alpha = \sum_{r=1}^{R} (\nu''_{\alpha,r} - \nu'_{\alpha,r}) \left[k_{f,r}(T) \sum_{s=1}^{N} X_s^{\nu'_{s,r}} - k_{b,r}(T) \sum_{s=1}^{N} X_s^{\nu''_{s,r}}\right]$$

The data compiled for our five-species calculations followed the reaction mechanism and the functional form of $k_{f,r}$, $k_{b,r}$ as suggested by Park.[12,13]

Relaxation of vibrational energy is modeled by

$$\dot{q}^\alpha = \frac{q^{*,\alpha}(T) - q^\alpha}{\tau^\alpha(p, T)}, \quad \alpha = 1, \ldots, N$$

where $q^{*,\alpha}(T)$ = equilibrium vibrational energy per unit mass of species $\alpha$ at temperature $T$ and $\tau^\alpha$ = relaxation time. The monatomic species do not possess vibrational modes, so $q^\alpha \equiv 0$ for $\alpha$ = monatomic species. These terms are given explicitly by[11]

$$q^{*,\alpha}(T) = \frac{R^\alpha \theta_0^\alpha}{\exp(\theta_0^\alpha/T) - 1}, \qquad \alpha = O_2, N_2, NO$$

where $\theta_0^\alpha$ = vibrational temperature for species $\alpha$ and

$$\tau^\alpha(p, T) = \frac{B^\alpha \exp[(k^\alpha/T)^{1/3}]}{p}$$

The equation for $\tau^\alpha$ is an approximate form of the Landau–Teller equation valid in the temperature range considered for this work.[11] The constants $B^\alpha$ and $k^\alpha$ must be experimentally determined; we use the data from Ref. 11 with the additional approximation that the heat bath molecule for species $\alpha$ is taken to be species $\alpha$ (in general, the constants depend on the collision partner).

### Characteristic Form

We rewrite the governing equations as a two-dimensional system in Cartesian coordinates, using our choice of five species of reacting air, as

$$\frac{\partial U}{\partial t} + \frac{\partial F(U)}{\partial x} + \frac{\partial G(U)}{\partial y} = S(U) \tag{2}$$

where the conservative variables $U$, fluxes $F(U)$ and $G(U)$, and the sources $S(U)$ are all vectors of length 12, which are derived straightforwardly from the expansion of Eqs. (1) in two space dimensions and for five species.

The nonconservative form of Eq. (2) is given formally by

$$V_t + AV_x + BV_y = \bar{S} \tag{3}$$

where $V = V(U)$ is a convenient set of nonconservative variables and the resulting matrices $A(V)$, $B(V)$ and the vector $\bar{S}$ are computed via

$$A = (\nabla_V U)^{-1}(\nabla_U F)(\nabla_V U)$$

$$B = (\nabla_V U)^{-1}(\nabla_U G)(\nabla_V U)$$

$$\bar{S} = (\nabla_V U)^{-1} S(U)$$

We denote the matrices of right and left, mutually orthogonal, eigenvectors associated with the matrix $A$ by $R_A$ and $L_A$, respectively. Similarly, $R_B$ and $L_B$ are the right and left, mutually orthogonal, eigenvectors associated with the matrix $B$. Denoting the velocity components in Cartesian coordinates by $\boldsymbol{u} = (u, v)$, the (ordered) eigenvalues of $A$ are $\lambda^1 = u - a$, $\lambda^2, \ldots, \lambda^{11} = u$, $\lambda^{12} = u + a$. The eigenvalues of $B$ are defined analogously with the substitution $u \rightarrow v$.

## Numerical Procedure

We start here with a description of the two-dimensional unsplit, hybrid IE Godunov scheme developed for the solution of flowfields with nonstiff sources. Then, we will discuss the appropriate extensions needed for the development of the stiff solver. The notation used later assumes a rectangular grid for simplicity; all of our computations are performed on such grids.

### Nonstiff Solver

The Godunov-like algorithms used here are predictor–corrector schemes. The second-order schemes compute time-centered edge fluxes that are consistent with the method of characteristics in the limit of weak waves and use nonlinear Riemann problems to enforce upwinding in the general case. The corrector step, which is a conservative difference, is given by

$$U_{j,k}^{n+1} = U_{j,k}^n - \alpha_x(F_{j+1/2,k}^{n+1/2} - F_{j-1/2,k}^{n+1/2}) - \alpha_y(G_{j,k+1/2}^{n+1/2} - G_{j,k-1/2}^{n+1/2}) + \alpha_t[S(U_{j+1/2,k}^{n+1/2}) + S(U_{j-1/2,k}^{n+1/2}) + S(U_{j,k+1/2}^{n+1/2}) + S(U_{j,k-1/2}^{n+1/2})] \tag{4}$$

where $\alpha_x = \Delta t/\Delta x$, $\alpha_y = \Delta t/\Delta y$, and $\alpha_t = \Delta t/4$. In Eq. (4), we are using $F(\cdot)$ and $G(\cdot)$ to denote numerical flux functions. We note that the time-centered sources at the four zone edges are averaged and the resulting averaged source is integrated in

time. This form is used following Pember[8] rather than simply using $\Delta t \cdot S(U^n_{j,k})$ as may be formally required (and was used by the authors in past work[9]).

The states $U^{n+1/2}_{j+1/2,k}$ and $U^{n+1/2}_{j,k+1/2}$ are computed by the predictor step; it consists of construction of time-centered Riemann problems at zone edges and the calculation of states and fluxes at the boundary. The predictor step is outlined next.

The construction of the predicted edge values and fluxes, $U^{n+1/2}_{j+1/2,k}$, $F^{n+1/2}_{j+1/2,k}$, etc., follows the implicit–explicit strategy of Refs. 2–4. The two-dimensional implementation of this construction is based on the explicit unsplit method of Ref. 14. Consequently, one has dependencies such as $U^{n+1/2}_{j+1/2,k}$ ($U^{n+1}$, $U^n$), and each time-step update involves the solution of a nonlinear system for $U^{n+1}$.

*Predictor Step*

The numerical fluxes may be given the functional form $F^{n+1/2}_{j+1/2,k} = \mathcal{F}(V^{n+1/2}_{j+1/2,k,L}, V^{n+1/2}_{j+1/2,k,R})$, $G^{n+1/2}_{j,k+1/2} = \mathcal{G}(V^{n+1/2}_{j,k+1/2,B}, V^{n+1/2}_{j,k+1/2,T})$, where $V^{n+1/2}_{j+1/2,k,M}$ represents time-centered solutions of the characteristic Eq. (3) just to the left (respectively, right) of the zone edge $x = x_{j+1/2}$ for $M = L$ (respectively, $M = R$), and the bottom and top states ($M = B$, $T$) are similarly defined; $\mathcal{G}$ may be obtained from $\mathcal{F}$ by interchange of the $x$, $y$ coordinates and associated velocities. Here, for example,

$$\begin{aligned} V^{n+1/2}_{j+1/2,k,L} &= T^x_L V^n_{j,k} - R_A D^S_{A,L} L_A B(V_y)^{n+1/2}_{j,k} + R_A D^S_{A,L} L_A \bar{S}(V^n_{j,k}) \\ V^{n+1/2}_{j+1/2,k,R} &= T^x_R V^n_{j+1,k} - R_A D^S_{A,R} L_A B(V_y)^{n+1/2}_{j+1,k} \\ &\quad + R_A D^S_{A,R} L_A \bar{S}(V^n_{j+1,k}) \end{aligned} \tag{5}$$

where $T^x_L$ and $T^x_R$ are intermediate state operators defined by

$$\begin{aligned} T^x_L &= I + \tfrac{1}{2} R_A D^E_{A,L} L_A (I - \alpha_x A)\Delta^x + R_A D^I_{A,L} L_A \delta^+_t \\ T^x_R &= I - \tfrac{1}{2} R_A D^E_{A,R} L_A (I + \alpha_x A)\Delta^x + R_A D^I_{A,R} L_A \delta^+_t \end{aligned} \tag{6}$$

and the operators used previously will be defined later. Terms such as $V^{n+1/2}_{j,k+1/2,T}$ and $T^y_T$, which are used in calculating fluxes in the $y$ direction, are defined analogously to Eqs. (5) and (6). The second term on the RHS of the previous equations is a characteristic projection, for example, see Ref. 16, and the numerical operator $\Delta^x$ denotes the limited slope formula.[15] The transverse derivatives are approximated by

$$(V_y)^{n+1/2}_{j,k} \approx \frac{\hat{V}^{n+1/2}_{j,k+1/2} - \hat{V}^{n+1/2}_{j,k-1/2}}{\Delta y} \tag{7}$$

where, for example, $\hat{V}^{n+1/2}_{j,k+1/2} = \mathcal{G}(\hat{V}^{n+1/2}_{j,k+1/2,B}, \hat{V}^{n+1/2}_{j,k+1/2,T})$. The data for the functional $\mathcal{G}$ are calculated using only the intermediate state operators in Eq. (5), ignoring the corner transport and chemistry terms, i.e.,

$$\hat{V}^{n+1/2}_{j,k+1/2,B} = T^y_B V^n_{j,k}$$

$$\hat{V}^{n+1/2}_{j,k+1/2,T} = T^y_T V^n_{j,k+1}$$

The diagonal matrices $D^E_{A,L}$, $D^I_{A,L}$, and $D^S_{A,L}$ are

$$(D^S_{A,L})_{\nu\nu} = \begin{cases} \Delta t/2 & \text{if } |\sigma^\omega_j| < 1 \\ \Delta t/2\sigma^\nu_j & \text{otherwise} \end{cases} \tag{8}$$

$$(D^I_{A,L})_{\nu\nu} = \begin{cases} 1 - 1/|\sigma^\nu_j| & \text{if } \sigma^\nu_j > 1 \\ 0 & \text{otherwise} \end{cases} \tag{9}$$

$$(D^E_{A,L})_{\nu\nu} = \begin{cases} 1 & \text{if } 0 < \sigma^\nu_j < 1 \\ 0 & \text{otherwise} \end{cases} \tag{10}$$

Here, $\sigma^\nu_j = \Delta t/\Delta x_j \lambda^\nu(V^n_j)$ is the local CFL number for the $\nu$th characteristic in the $j$th zone. The diagonal matrices $D^E_{A,R}$, $D^I_{A,R}$, and $D^S_{A,R}$ are defined analogously to Eqs. (8–10) with the substitution $\sigma^\nu_j \to -\sigma^\nu_{j+1}$. Similarly, the diagonal matrices associated with the matrix $B$ are defined for the $y$ direction and are indicated with a $B$ subscript. Also, $L_A$, $L_B$, $R_A$, and $R_B$ are the matrices of left and right eigenvectors associated with the matrix indicated by the subscript. The finite difference operator $\delta^+_t$ is defined by $\delta^+_t V^n_{j,k} = V^{n+1}_{j,k} - V^n_{j,k}$. A similar procedure is followed to compute the states on the other three edges of each zone.

*Flux Function*

The corrector step described by Eq. (4) [and Eq. (17)] requires the definitions of two objects: 1) the time-centered state $U^{n+1/2}$ and 2) the numerical flux function $F = \mathcal{F}(U_L, U_R)$. In this work we used two different approaches for the two test problems:

1) For the doubly periodic shear layer, an Engquist–Osher (E–O) flux function (as implemented in Ref. 3) was used for the numerical flux and the time-centered state was computed based upon the approximate Riemann problem solution given by the E–O wave decomposition.

2) For the case that involves the creation of a shock wave, we used the Godunov flux and the Godunov time-centered state as computed using a scheme similar to the one described in Ref. 16 with four secant iterations for the calculation of the intersection of the wave curves.

*Nonlinear Solver*

The corrector step in Eq. (4) can be rewritten as

$$U^{n+1}_{j,k} + \alpha_x \Delta F(U^{n+1}_{j,k}) + \alpha_y \Delta G(U^{n+1}_{j,k}) - \alpha_t \tilde{S}(U^{n+1}_{j,k}) = U^n_{j,k} \tag{11}$$

where $\Delta F$ and $\Delta G$ are the flux differences, $\tilde{S}$ represents source averaging in Eq. (4), and dependencies on $U^n$ are suppressed. Equation (11) can be expressed in the form

$$U^{n+1} = g(U^{n+1}) \tag{12}$$

where $U^{n+1} = \{U^{n+1}_{j,k}\}$ is the vector of unknowns and $g$ is the obvious rearrangement of Eq. (11). The solution of Eq. (12) is obtained by the use of a special acceleration procedure based upon either a Jacobi iteration or a Gauss–Seidel iteration with red–black ordering. This procedure was implemented in past work by Collins[3] (for the nonreacting case) and found to produce satisfactory results. The special acceleration iteration for Eq. (12) is

$$\begin{aligned} &U^{n+1,0} = U^n, \quad U^{n+1,\nu+1} = \Theta g(U^{n+1,\nu}) + (I - \Theta)U^{n+1,\nu} \\ &\qquad \nu = 0, 1, \ldots, \end{aligned} \tag{13}$$

where the matrix $\Theta$ is a diagonal matrix consisting of the acceleration parameters. Since each $12 \times 12$ block along the diagonal of $\Theta$ is associated with one computational zone, then $\Theta = \{\Theta_{j,k}\}$, where each $\Theta_{j,k} \in \mathcal{R}^{12\times 12}$. Each $\Theta_{j,k}$ is defined by

$$\Theta_{j,k} = \frac{1}{\max(1, \sigma^n_{j,k})} I \tag{14}$$

with $\sigma^n_{j,k}$ defined as the maximum of all local CFL numbers for zone $(j, k)$. If this number is less than 1, then the previous procedure reduces to solving for the explicit solution, i.e., the scheme reduces to the explicit Godunov scheme.

**Stiff Solver**

The modifications to the scheme for stiff source terms follow some of the general ideas discussed by Yee,[7] Lafon and Yee,[5] LeVeque and Yee,[6] and, more specifically, by Pember,[8] who studied the problem of stiffness in the context of the second-order, explicit Godunov scheme for single-source term systems satisfying the subcharacteristic condition.

Theoretically, one can split the sources into a nonstiff part $S(U)$, and stiff part $H(U)$, and use only the stiff part in the procedure to be discussed later. However, from a practical point of view, it may require additional work to examine the sources every time step and split them into their stiff and nonstiff counterparts. Moreover, in some applications, it is not at all clear how to do that, for example, two-phase flows mixed with chemistry. Referring to Eq. (2), make the replacement $S(U) \leftarrow S(U) + H(U)$, where $H(U)$, $S(U)$ represent the stiff and nonstiff sources, respectively (this notation follows Ref. 8). Assuming, a priori, that all sources are stiff, it is useful to rename the sources by $H(U)$, and Eq. (2) is replaced by

$$\frac{\partial U}{\partial t} + \frac{\partial F(U)}{\partial x} + \frac{\partial G(U)}{\partial y} = H(U) \tag{15}$$

The modifications required to solve Eq. (15) relative to our algorithm described previously for Eq. (2) are discussed next. For simplicity, we do not discuss the general case where both $S(U)$ and $H(U)$ are nonzero; also, our numerical results solve either Eq. (2) or (15) as appropriate.

*Predictor Step*

We replace the initial data in Eq. (5) by

$$\begin{aligned} V^{n+1/2}_{j+1/2,k,L} &= T^x_L V^n_{j,k} - R_A D^S_{A,L} L_A B(V_y)^{n+1/2}_{j,k} \\ &\quad + R_A D^S_{A,L} L_A \bar{H}(V^{n+1/2}_{j+1/2,k,L}) \\ V^{n+1/2}_{j+1/2,k,R} &= T^x_R V^n_{j+1,k} - R_A D^S_{A,R} L_A B(V_y)^{n+1/2}_{j+1,k} \\ &\quad + R_A D^S_{A,R} L_A \bar{H}(V^{n+1/2}_{j+1/2,k,R}) \end{aligned} \tag{16}$$

so that the stiff sources are treated semi-implicitly in the characteristic projection step. For the explicit scheme, the solution of Eqs. (16) is obtained using an inner iteration decoupled from the iteration loop (for the implicit sources) in the corrector step. For the implicit–explicit scheme, this is one option among others; see further discussion in the Results section.

*Corrector Step*

Here, we replace Eq. (4) by

$$\begin{aligned} U^{n+1}_{j,k} &= U^n_{j,k} - \alpha_x[F(U^{n+1/2}_{j+1/2,k}) - F(U^{n+1/2}_{j-1/2,k})] \\ &\quad - \alpha_y[G(U^{n+1/2}_{j,k+1/2}) - G(U^{n+1/2}_{j,k-1/2})] + \Delta t H(U^{n+1}_{j,k}) \end{aligned} \tag{17}$$

The resulting equations for the predictor and corrector steps are then implicit even if all characteristics are treated explicitly. This update is (formally) only first-order accurate in time. However, it is argued in Ref. 8 that, as the relaxation times approach zero, the time-stepping procedure becomes second-order accurate; see Ref. 8 for problems with longer relaxation times and appropriate discretization strategies. The fluxes and interface values are computed for stiff source problems exactly as described for nonstiff sources in the preceding section.

*Discussion*

Note that the acoustic modes are intended to be treated implicitly by the scheme for low Mach number flows. For this case, there appears to be no mechanism by which the variation of sound speed with respect to chemistry or relaxation can affect the validity of our extension of the (gasdynamics) scheme in Refs. 3 and 4. However, issues are raised by using the extended scheme for flows with near sonic regions that are being treated explicitly. In particular, as the speed of sound varies quickly, especially in the stiff case, over small spatial regions, the flux computed by the explicit scheme will either reduce to first-order accuracy or, conceivably, lead to spurious oscillations if the subsonic/supersonic variation takes place at or near the mesh scale. Pember[8] has proposed changes in the second-order Godunov procedure (including a redefinition of the characteristic projection and the implementation of a more restrictive slope limiter) for stiff relaxation. We note that gasdynamics with vibrational nonequilibrium but no chemistry is indeed a system of conservation laws with relaxation, which satisfies the subcharacteristic condition[8]; however, full chemically reacting systems maintain both increases and decreases of the sound speed with respect to the reaction progress variables (e.g., dissociation or recombination), which implies that the subcharacteristic condition is not satisfied in general. Although we have experimented with some of the proposals in Ref. 8 and have obtained minor variations in the solutions, the results presented next already validate the new methodology in principle. We remark that, even for the special case of vibrational nonequilibrium but no chemistry, we cannot absolutely guarantee that, as the sources approach equilibrium, the flux approximates an upwind flux for the equilibrium system. In particular, optimization of the flux function for both nonequilibrium chemistry models is still open.

The implicit nature of the stiff predictor and its interaction with the overall implicit–explicit methodology is a significant numerical analysis problem only touched upon here. For example, optimal convergence rates and acceleration parameters depend on the stiffness of the problem at hand.

## Numerical Results

Two model problems have been tested in some detail. The first is a low Mach number doubly periodic inviscid shear layer (see Fig. 9.1 in Ref. 3; also see Ref. 9). Our calculations and the results presented here focus on the early time onset of nonlinear convective instability coupled with the nonequilibrium relaxation processes. The late-time large-scale vortex rollup characteristic of this problem[3] takes place under near-equilibrium conditions and, therefore, is not of interest here. The maximum CFL number for all calculations of this subsonic problem is always constrained by setting the particle characteristic CFL number to be 0.9; with the exception of further startup restraints (described later), the IE code is run without further restraint and actual CFL ranges are also recorded later.

The second is a simulation of jet injection into a supersonic transverse flow, which involves the creation of a shock wave and the mixing of two jets as described in Ref. 17. The study[17] focuses on the interaction between a gas jet that contains particles and an external particle-free stream. Our objectives here are to test our (chemically reacting) stiff source coupling in a realistic application (plumes and combustor environments are other examples) and to lay the groundwork for a future implementation of an analogous code designed to solve for multiphase, chemically reacting flows.

**Doubly Periodic Shear Layer**

The initial velocity field $\boldsymbol{u} = (u, v)$ is scaled to match the previously studied nondimensional single species nonreactive calculations.[3] To study the origins of stiffness and the associated numerical difficulties, each flowfield was solved using three reaction models: 1) frozen, 2) vibrational relaxation only, and 3) full (five-species chemistry/vibrational relaxation) chemistry. The frozen results are not discussed here (they were used only for code validation). The initial conditions are

$$\begin{gathered} \bar{u} = \begin{cases} \tanh[30(\bar{y} - 0.25)] & \text{if } \bar{y} \le 0.5 \\ \tanh[30(0.75 - \bar{y})] & \text{if } \bar{y} > 0.5 \end{cases} \\ \bar{v} = 0.05 \sin 2\pi\bar{x} \\ p = \begin{cases} \bar{p} & \text{if } 0.25 \le \bar{y} \le 0.75 \\ 1.05\bar{p} & \text{elsewhere} \end{cases} \\ \rho = 2.25 \times 10^{-6} \text{ g/cc} \\ c_{O_2} = 0.23, \qquad c_{N_2} = 0.77 \\ q^\alpha = 0.0, \qquad \alpha = O_2, N_2, NO \end{gathered} \tag{18}$$

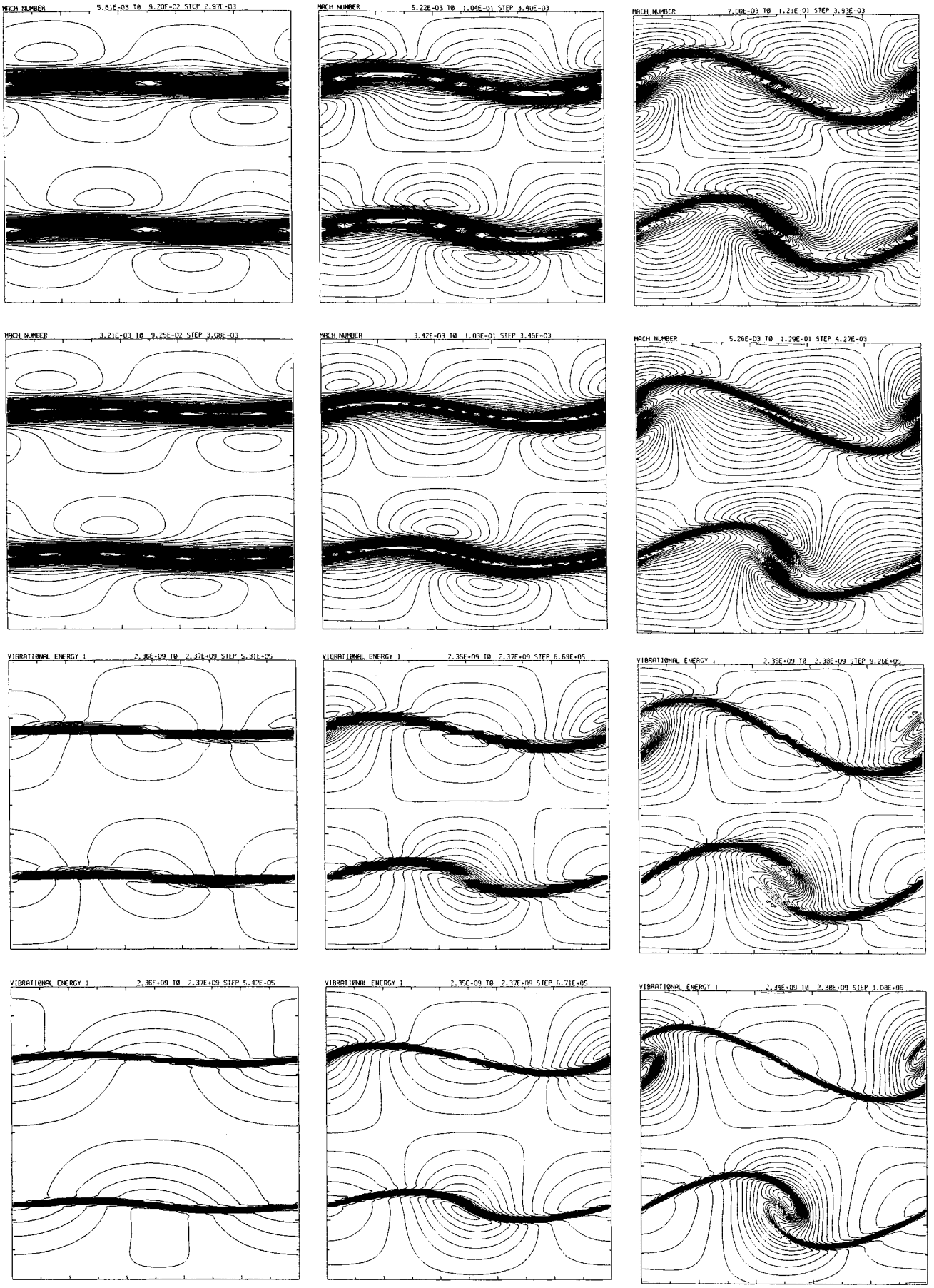


**Fig. 1 Doubly periodic shear layer, 2100 K, vibrational relaxation flow solution: contour plots of (top to bottom) Mach number on a 64 × 64 and a 128 × 128 grid, and $O_2$ specific vibrational energy on a 64 × 64 and a 128 × 128 grid, at (from left to right) $T$ = 0.5, 1.0, and 1.5 s.**

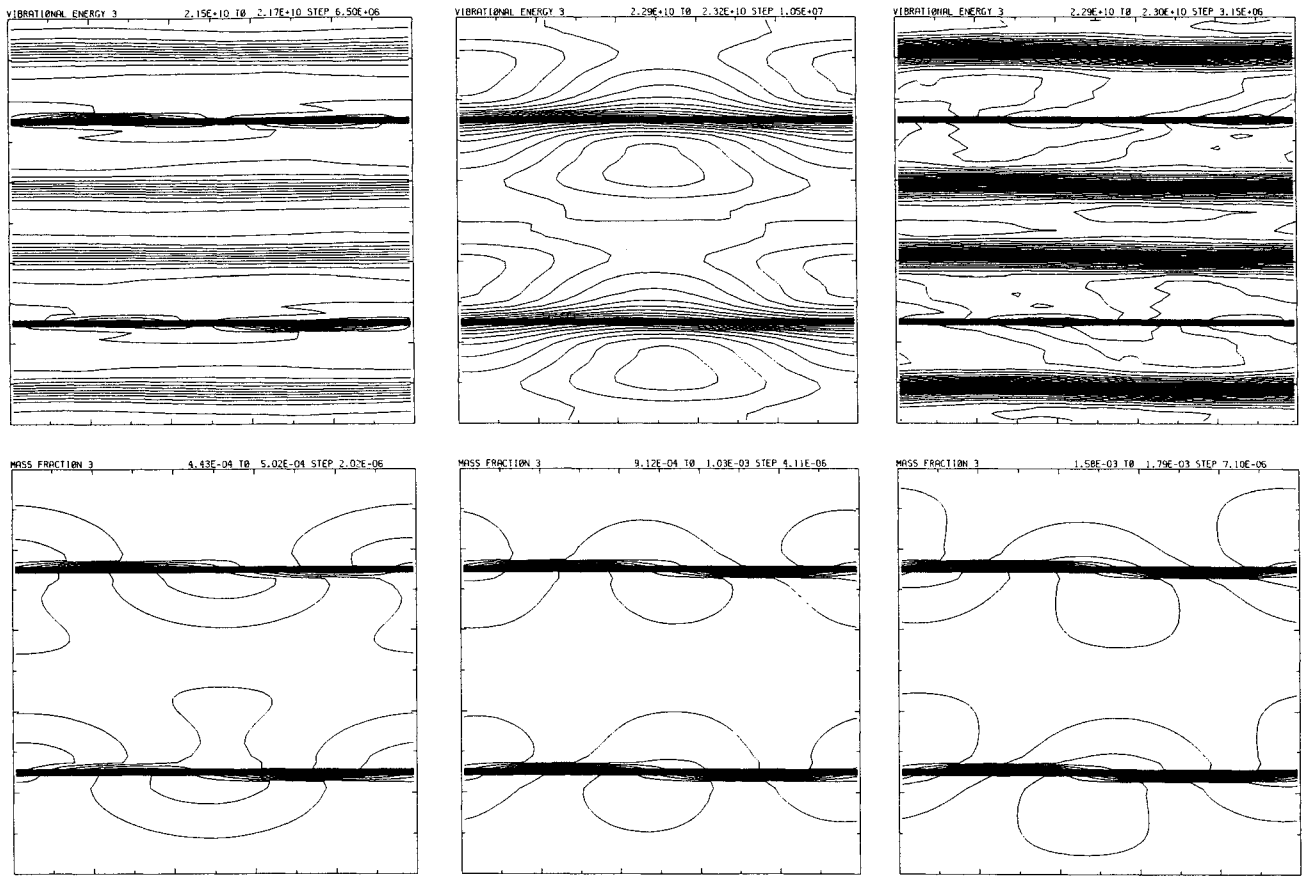


**Fig. 2 Doubly periodic shear layer, 3100 K, chemically reacting flow solution: contour plots of NO (from top to bottom) specific vibrational temperature and mass fraction at (from left to right) $T$ = 0.05, 0.075, and 0.1 s.**

where $\bar{u} = u/u_{\max}$, $\bar{v} = v/u_{\max}$, $\bar{y} = y/x_{\max}$, $\bar{x} = x/x_{\max}$, $u_{\max} = 7500$ cm/s, and $x_{\max} = 7500$ cm. The initial pressure in the center jet $\bar{p}$ is given by 1.35 or $2.00 \times 10^4$ dyne/cm$^2$ for the calculations discussed here, with corresponding initial air temperatures of 2100 or 3100 K. The maximum flow Mach number is about 0.1 as the calculations begin. Results for the 2100 K initial data using the vibrational relaxation only model and for the 3100 K initial data using both reactive flow models are discussed in detail.

Vibrational relaxation of $O_2$ is the stiffest reaction at both temperatures for the results using the vibrational relaxation-only model [with the initial conditions (18)], leading to large reaction rates that quickly reduce the temperature and relax the system close to vibrational equilibrium where it remains; indeed, equilibrium is reached prior to $T = 0.1$ for both calculations. In more detail, the vibrational energy relaxation times $\tau^{\alpha}$ for $O_2$ and $N_2$ are $3 \times 10^{-4}$ and $9 \times 10^{-3}$ s, respectively, for the 2100 K results, and are $5 \times 10^{-5}$ and $2 \times 10^{-3}$ s, respectively, for the 3100 K results. The reactions cause a drop in the temperature of about 250 K (2100 K data) and 530 K (3100 K data). Thus, the system is very stiff for both sets of initial data during the initial transient.

The 2100 K IE calculation using the vibrational relaxation model and the nonstiff solver fails (i.e., the stiff energy mode accumulates large errors leading to an unstable calculation) even upon starting with a very low max CFL number of about 0.05, so that the source integration step is small, and slowly increasing it (by 2% every step) to 0.9 fails to produce a solution. On the other hand, for calculations with the stiff solver, numerically stable transients were obtained with the initial CFL set to 1.1 and increased each time step by 5% until the scheme's natural CFL (8.5–10.5 here) takes over.

The contours of Mach number and $O_2$ specific vibrational energy at times $T$ = 0.5, 1.0, and 1.5 s are shown in Fig. 1. The results are shown on $64 \times 64$ and $128 \times 128$ grids (which serve to validate the coarse grid results prior to significant rollup). The solutions are smooth and it is clear that the vibrational energies (and temperature, not shown here) reached (chemical) equilibrium values at a time $T < 0.5$ and their amplitudes remain almost constant thereafter. The solution shown in Fig. 1 is nevertheless different from the frozen flow solution (not shown here); the reactions cause a drop in the temperature (of about 250 K), hence, changing the dynamics and evolution rates of the variables, for example, Mach number and pressure.

As expected, the 3100 K IE calculation using the vibrational relaxation model and the nonstiff solver also fails (and much sooner than the 2100 K case, even with initial CFL numbers as low as 0.01). Using the stiff solver coupled with the IE scheme at $T = 0$ is also unstable. Thus, a two-stage strategy was implemented, using the (modified, see later) stiff solver throughout: 1) for $0 < T < 1$, the calculation is explicit and 2) at $T = 1$, the full IE scheme is used. The solution at $T = 0.1$ displays good resolution even on a coarse $64 \times 64$ grid (not shown). Here, a relatively small initial CFL number of 0.1 is used that gradually increases to 0.9. This stage of the calculation is relatively expensive, requiring 25 iterations in the corrector step and 20 in the predictor step with relaxation factors of 0.1 for both cycles. Upon commencement of the second stage of the calculation, the CFL number begins to increase immediately from 0.9 to the scheme's natural range (10.5–12 here); the code imposed a modest restraint on CFL growth over each time step. Since the initial transient is gone at $T = 0.1$, the stiff solver can be modified by implementing the nonstiff predictor in place of the stiff predictor step iteration cycle while the stiff corrector step is retained. The calculation remains stable up to completion at $T = 1.5$ and the amplitudes of the thermodynamic variables, specifically the vibrational energies, remain nearly constant. Note that the shear layer rollup has just begun at $T = 1.5$ (the extent is comparable to that depicted in Fig. 1 at $T = 0.5$).

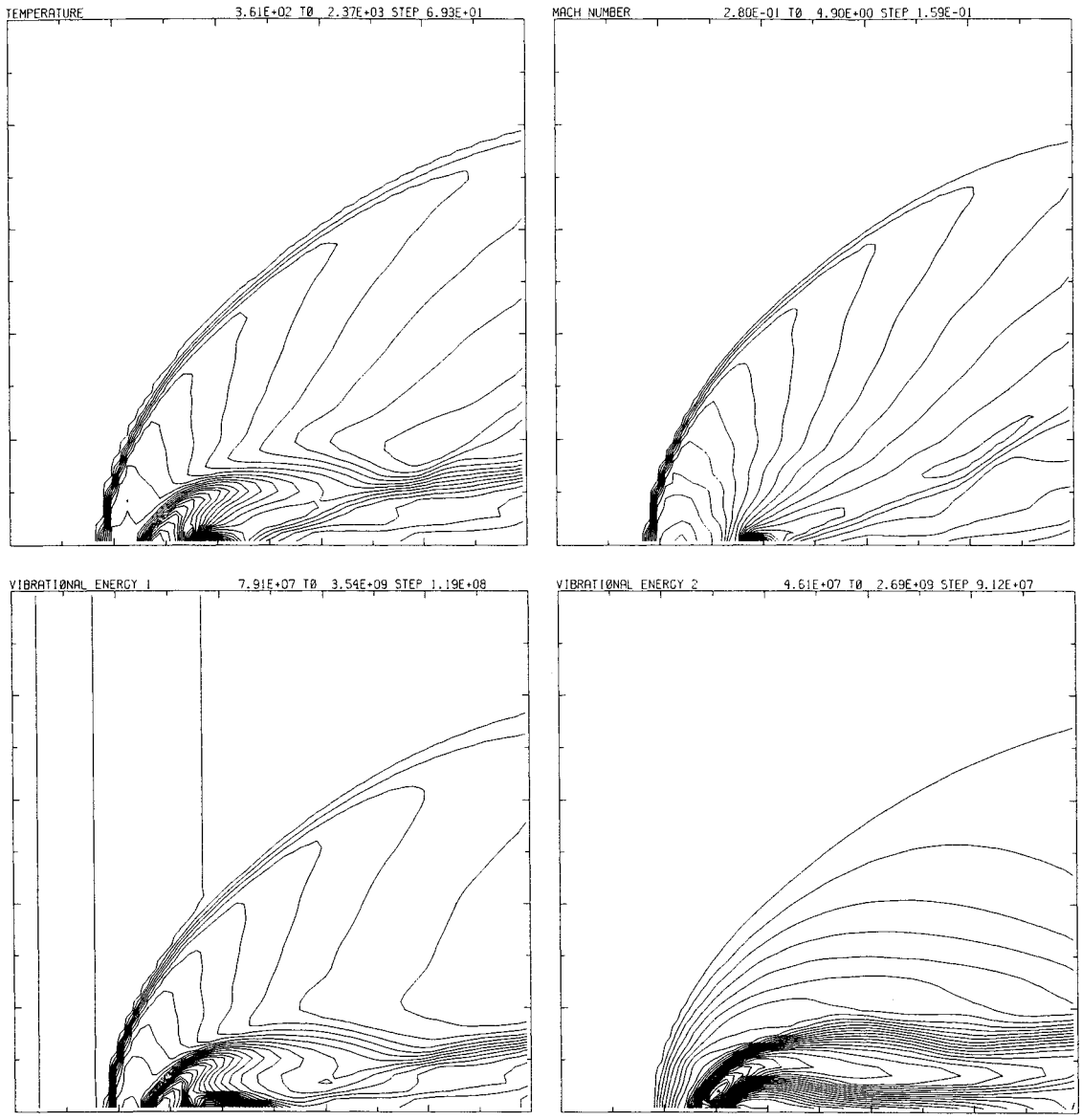


**Fig. 3 Transverse injection of a jet, vibrational relaxation flow solution: contour plots of (from left to right, top to bottom) temperature, Mach number, and specific vibrational energies of $O_2$ and $N_2$ at $T = 0.001$ s.**

The 3100 K full chemistry model problem results in an even stiffer transient. The two molecules present at $T = 0$ dissociate quickly and the resulting atoms recombine to form NO; the rates are about $8 \times 10^{-6}$ s, which is faster than the relaxation modes, and the coupling with the other chemical reactions is stronger. Consequently, the calculation for this problem is much harder. The initial CFL number is set at 0.05 and it is gradually increased to about 0.65 (and so it is fully explicit); the stiff solver is used. It is found that the iteration parameters needed to solve the nonlinear systems that arise from the predictor and corrector steps are strongly dependent upon the CFL number; as the CFL number increases more iterations and smaller relaxations factors are needed for convergence. Contour plots of the specific vibrational energy and mass fraction of NO at $T = 0.05$, 0.075, and 0.1 s are displayed in Fig. 2. The initial temperature of about 3100 K has dropped quickly, and at $T = 0.05$ s it is already at 2550 K; from then on it changes very slowly. The specific vibrational energy of NO rises and reaches a local maximum at $T = 0.075$ s and drops slightly at later times. The amplitude of the mass fraction of NO and the other species (not displayed in Fig. 2) reflect the much slower evolution of the chemical dissociation and recombination compared to the vibrational relaxation rates; in particular, chemical equilibrium is clearly not achieved at $T =$ 0.1. As in the vibrational relaxation case, the flowfield evolves at a much slower rate and the shear layer is barely distorted.

### Transverse Injection of Fluid in Supersonic Flow

The geometry of this two-dimensional simulation follows.[17] A rectangular $64 \times 64$ mesh is used; the wall has a length of 1.0 m and the injection slot extends from 0.25 to 0.35 m. The freestream Mach number is 2.0, while the injected gas jet is sonic. The initial pressure is 1.0 atm in the gas and 2.5 atm in the jet. Also, $\rho = 0.41 \times 10^{-3}$ gm/cc, $c_{O_2} = 0.23$, $c_{N_2} = 0.77$, $q^\alpha = 0.0$, $\alpha = O_2$, $N_2$, and NO for both the gas and jet flow at $T = 0$. Note that the flow is supersonic and that the CFL condition must be satisfied for all characteristic fields so that the calculations are explicit.

The vibrational relaxation only calculation is considered first. The temperature of the gas is 845 K and the jet temperature is 2113 K. The maximum CFL number was set to 0.9 with an initial CFL number of 0.5. The nonstiff solver could not solve the problem, even using initial CFL numbers as low as 0.01 with very small increments per time step allowed. With the stiff solver, relaxation parameters of 0.1 (50 iterations) in the corrector step and 0.05 (20 iterations) in the predictor step were chosen. Tests using larger relaxation factors failed after several tens of time steps. Contour plots of temperature, Mach

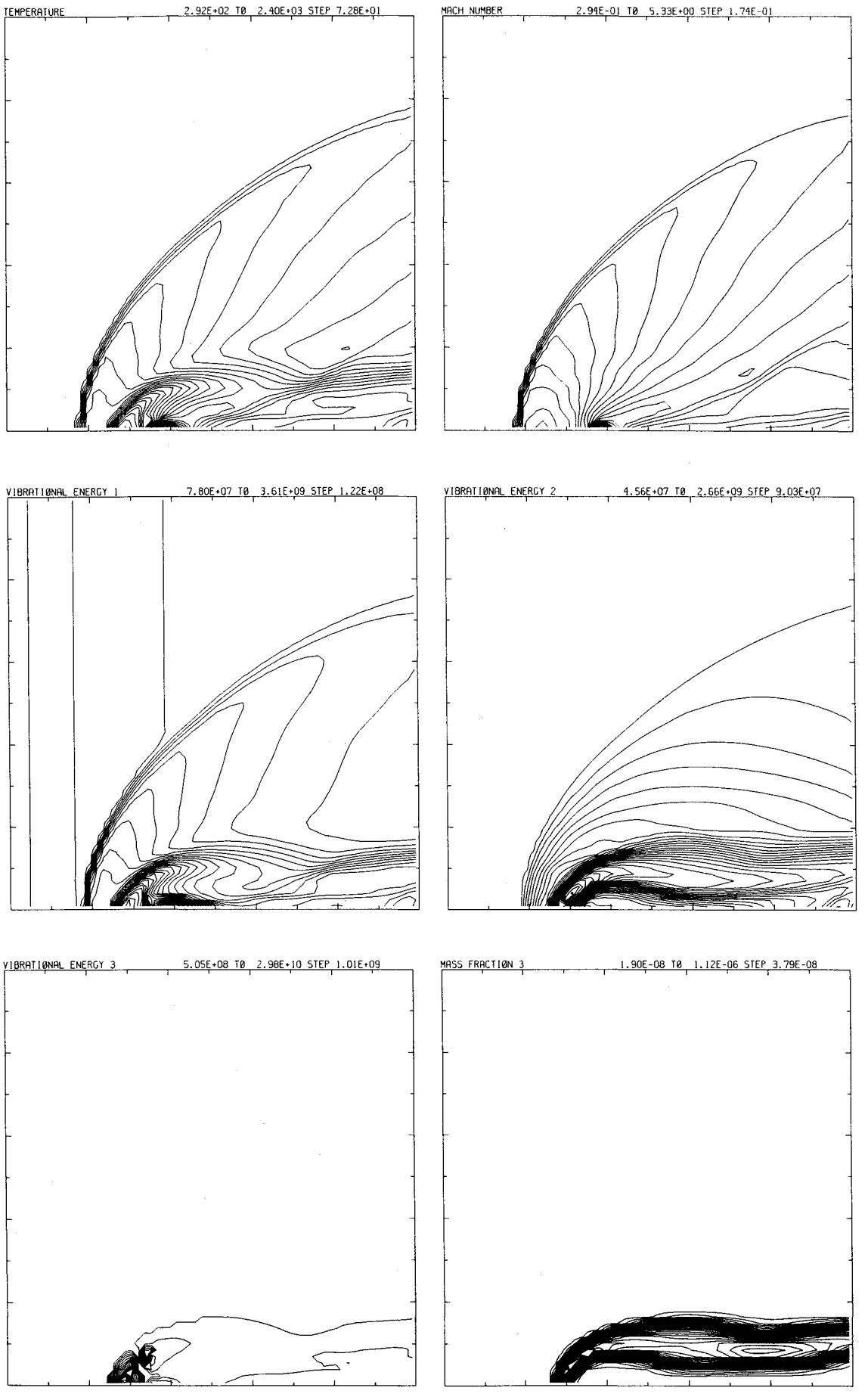


**Fig. 4 Transverse injection of a jet, chemically reacting flow solution: contour plots of (from left to right, top to bottom) temperature, Mach number, specific vibrational energies of $O_2$, $N_2$, and NO, and NO mass fraction at $T = 0.001$ s.**

number, and specific vibrational energies of the $O_2$ and $N_2$ molecules at $T = 0.001$ s are displayed in Fig. 3; the temperature reaches a maximum of 2370 K, the flow expands to a maximum Mach number of $M = 4.9$, and the relaxation of the vibrational energies of $O_2$ and $N_2$ molecules is resolved nicely.

For the full chemically reacting model, the flowfield involves disparate evolution rates of the different species and is the most difficult case to compute. Only the stiff solver was used. The maximum CFL was set to 0.4 and the initial CFL was 0.1; relaxation parameters of 0.1 (50 iterations) in the corrector step and 0.001 (40 iterations) in the predictor step were chosen. We found, via other tests, that the predictor iteration cycle is very sensitive to the relaxation parameters we use; using larger relaxation factors (results not shown here) can result in nonphysical values for the stiffest vibrational mode (NO) and the stiffest reactions (those involved in the creation of N), which eventually results in large errors propagating through all of the thermodynamic variables. Contour plots of temperature, Mach number, specific vibrational energies of the three molecules, and NO mass fraction are shown in Fig. 4 at $T = 0.001$ s.

## Summary and Conclusions

The unsplit explicit and implicit–explicit Godunov methodologies have been successfully extended to treat stiff, nonequilibrium, chemically reacting flowfields. This is done using a completely unsplit operator: the integration of the spatial derivatives and the source terms are fully coupled. For the fully explicit mode of the scheme, the procedure used allows for the formal retention of second-order accuracy of the numerical scheme.

The stiff and nonstiff solvers developed here were used to solve two unsteady flow cases: a doubly periodic, unstable, low Mach number shear-layer flow and the simulation of the evolution of a shock wave caused from the transverse injection of fluid into supersonic flow. Our results demonstrate that 1) the extended IE method has the capability of producing high-resolution computations, 2) the method converges, and 3) the new stiff solver can handle more difficult problems than the nonstiff solver.

It is also shown that, after the initial transient is resolved (perhaps using the explicit solver), the computed solution remains close to local thermodynamic equilibrium and can be stably advanced in time using the more efficient implicit–explicit method.

Our scheme is one of the few available that is capable of computing high-resolution simulations on grids with associated fluid dynamic time steps that are significantly larger than the stiff chemistry time step. Several aspects of the code (which are all coupled), can be further optimized; for example, 1) implementing faster nonlinear solvers (e.g., multigrid acceleration, see Ref. 3 for the frozen case) and 2) developing a reliable automatic switch from fully explicit to IE during the transient. A major open issue is the construction of an optimal flux function for stiff flowfields. For most practical applications, it would be more efficient to implement our scheme in the context of adaptive mesh refinement so that the stiffest flowfield regions can be assigned a finer mesh; we expect this to be reasonably straightforward.

## Acknowledgments

The support of NASA Ames Research Center under SBIR Contract NAS2-13798(CDT), the National Science Foundation under SBIR Grant ISI-8960133 and Grant DMS-8703971, and the support of the Defense Nuclear Agency under DNA MIPR#93-540 and DNA001-91-C-0095 are acknowledged with thanks. All computations discussed here were performed on the CRAY C90 at NASA Ames Research Center and we thank the Center for their generous support.

## References

[1]Fryxell, B. A., Woodward, P. R., and Colella, P., "An Implicit-Explicit Hybrid Method for Lagrangian Hydrodynamics," *Journal of Computational Physics*, Vol. 63, No. 2, 1986, pp. 283–310.

[2]Collins, J. P., Colella, P., and Glaz, H. M., "An Implicit-Explicit Eulerian Godunov Scheme for Compressible Flow," *Journal of Computational Physics*, Vol. 116, No. 2, 1995, pp. 195–211.

[3]Collins, J. P., "Implicit/Explicit Godunov Schemes for Unsteady Gas Dynamics," Ph.D. Dissertation, Univ. of Maryland, Dept. of Mathematics, College Park, MD, 1992.

[4]Collins, J. P., Colella, P., and Glaz, H. M., "An Unsplit Implicit-Explicit Godunov Method for Compressible Gas Dynamics," *Proceedings of the 1st European CFD Conference*, edited by C. Hirsch, Vol. 2, Elsevier, Amsterdam, 1992, pp. 659–666.

[5]Lafon, A., and Yee, H. C., "On the Numerical Treatment of Nonlinear Source Terms in Reaction-Convection Equations," AIAA Paper 92-0419, Jan. 1992.

[6]LeVeque, R. J., and Yee, H. C., "A Study of Numerical Methods for Hyperbolic Conservation Laws with Stiff Source Terms," NASA TM-100075, March 1988.

[7]Yee, H. C., and Shinn, J. L., "Semi-Implicit and Fully Implicit Shock-Capturing Methods for Hyperbolic Conservation Laws with Stiff Source Terms," *AIAA Journal*, Vol. 27, No. 3, 1989, pp. 299–307.

[8]Pember, R. B., "Numerical Methods for Hyperbolic Conservation Laws with Stiff Relaxation II. Higher Order Godunov Methods," *SIAM Journal on Scientific and Statistical Computing*, Vol. 14, No. 4, 1993, pp. 824–859.

[9]Krispin, J., and Glaz, H. M., "Nonequilibrium, Chemically Reacting Flowfields and the Implicit-Explicit Godunov Scheme," *Proceedings of the 13th International Conference on Numerical Methods in Fluid Dynamics* (Rome, Italy), edited by M. Napolitano and F. Sabetta, Springer–Verlag, Heidelberg, 1992, pp. 330–334.

[10]Park, C., "Radiation Enhancement by Nonequilibrium in Earth's Atmosphere," *Journal of Spacecraft and Rockets*, Vol. 22, No. 1, 1985, pp. 27–36.

[11]Vincenti, W. G., and Kruger, C. H., *Introduction to Physical Gas Dynamics*, Krieger, Malabar, FL, 1975.

[12]Park, C., "On Convergence of Computation of Chemically Reacting Flows," AIAA Paper 85-0247, Jan. 1985.

[13]Park, C., "Problems of Rate Chemistry in the Flight Regimes of Aeroassisted Orbital Transfer Vehicles," *Thermal Design of Aeroassisted Orbital Transfer Vehicles*, edited by H. F. Nelson, Vol. 96, Progress in Astronautics and Aeronautics, AIAA, New York, 1985, pp. 511–537.

[14]Colella, P., "Multidimensional Upwind Methods for Hyperbolic Conservation Laws," *Journal of Computational Physics*, Vol. 87, No. 1, 1990, pp. 171–200.

[15]Colella, P., "A Direct Eulerian MUSCL Scheme for Gas Dynamics," *SIAM Journal on Scientific and Statistical Computing*, Vol. 6, No. 1, 1985, pp. 104–117.

[16]Colella, P., and Glaz, H. M., "Efficient Solution Algorithms for the Riemann Problem for Real Gases," *Journal of Computational Physics*, Vol. 59, No. 2, 1985, pp. 264–289.

[17]Hosangadi, A., Sinha, N., Dash, S. M., and York, B. J., "Progress Towards the Analysis of Transient Combustion, Multi-Phase Flows Using Upwind/Implicit Numerics," AIAA Paper 93-0238, Jan. 1993.